STUDIES OF THE CHEMICAL COMPOSITION OF COSMIC RAYS WITH $Z = 3$–30 AT HIGH AND LOW ENERGIES*

W. R. WEBBER, S. V. DAMLE, and J. KISH
Physics Department, University of New Hampshire, Durham, N.H., U.S.A.

(Received 18 October, 1971)

Abstract. We have measured the chemical composition of cosmic rays with $Z \geqslant 2$ over an energy range from ~ 100 MeV/nuc to > 2 GeV/nuc using 2 new large area counter telescopes. One of these instruments was a 4 element $dE/dx \times E \times$ Range telescope, the other a 4 element $dE/dx \times$ Cerenkov $\times$ $\times$ Range telescope. Two balloon flights with these telescopes at Ft. Churchill in the summer of 1970 provided a total of nearly 1000 Fe nuclei with a charge resolution ranging from ~ 0.10 charge unit at Carbon to ~ 0.25 charge unit at Fe. A detailed charge spectrum is obtained at both high and low energies. Some important differences exist between the present results and those obtained earlier, due in part to the improved statistical accuracy and in part to the improved background rejection of the present data. In particular, the abundance of Cr and Mn are each found to be $\sim 0.10 \times$ Fe in contrast to the earlier ratio of ~ 0.30 found by some workers for each of these nuclei. The abundance of these two nuclei, as well as others in the 15–25 range, shows no strong dependence on energy. We have extrapolated our composition data to the cosmic ray sources using a variety of interstellar path length distributions. The abundances of *all* secondary nuclei with Z between 3–25 are consistent only with propagation models which have vacuum path length distributions which do not differ greatly from exponential. The source abundances of nuclei with $Z = 15$, 17, 18, 19, 21, 22, 23, 24, and 25 are found to be $< 0.02 \times$ Fe. For the remaining nuclei, Na, Al, S, and Ca are found to have source abundances of 0.07, 0.11, 0.18 and 0.13 of Fe respectively. The source abundance of C and O relative to Fe is also much different than some earlier compilations. A comparison of solar and cosmic ray abundances reveals certain selective differences, rather than a systematic overabundance of heavy nuclei in cosmic rays, as has been suggested in the past. These differences are discussed in terms of a common nucleosynthesis origin of the two species of particles.

1. Introduction

In the summer of 1970 we carried out measurements from Ft. Churchill, Canada to determine the absolute intensity, charge composition, and energy spectrum of primary cosmic rays with $Z = 2$–30 using two new balloon borne particle telescopes. These two telescopes enabled us to cover the energy range from the atmospheric cut-off at 2.2 g cm^{-2} depth to approximately 1.5 GeV/nuc for the above charges and provided energy spectra in overlapping energy ranges, enabling the intensities determined by two different techniques to be compared. Over all, these measurements represent a considerable improvement, both statistically and in terms of charge and energy resolution, over our previous measurements of these charges (von Rosenvinge *et al.*, 1969; Lezniak *et al.*, 1970). In this paper we shall be principally interested in the charge composition of the primary cosmic rays, and will consider the composition in two energy ranges: $>$ 850 MeV/nuc and 250–850 MeV/nuc.

* Research sponsored by the National Aeronautics and Space Administration under Grant No. NGR-30-002-052.

Astrophysics and Space Science **15** (1972) 245–271.

Our current understanding of the charge composition of primary cosmic rays has been summarized in a fine review article by Shapiro and Silberberg (1970), (SS). These authors have also presented detailed fragmentation parameters appropriate to the propagation of the cosmic rays through interstellar hydrogen and have estimated the source abundances of these particles considering various possibilities for the propagation through interstellar space. Individual high resolution studies covering the entire charge spectrum between $Z=2$–26 are few. We may mention the work of the Danish-French group at high energies (Casse *et al.*, 1971), and the Chicago satellite results at low energies (Cartwright *et al.*, 1971). Both of these observations have a resolution comparable to ours but considerably less statistical accuracy.

The charge composition of the primary cosmic radiation that we measure differs in many important respects from that summarized by SS, as well as the latest revised compilation by these authors (Shapiro and Silberberg, 1971). Since the statistical accuracy of our results considerably exceeds that of all the data used in the SS survey, we are able to determine the cosmic ray source abundances to a precision of ± 0.02 of the Fe abundance – subject to uncertainties in the fragmentation parameters. This is sufficient to provide a basis for a fairly detailed comparison of cosmic ray source abundances with so-called cosmic and/or solar abundances, and abundances predicted on the basis of more quantitative recent ideas of nucleo-synthesis.

In addition, we are able to study the effects of the interstellar propagation on the cosmic ray charge composition in detail. Particular attention is paid to the relative production of secondary nuclei of different charge on the model chosen for interstellar propagation. The ability of this type of data to select between the various propagation models is examined, and it is concluded that the vacuum path length distribution of the cosmic rays in interstellar space must be quite closely an exponential function.

2. Instrumentation and Balloon Flights

The data to be presented here was obtained on balloon flights in the summer of 1970 using two different instruments. These instruments had much larger geometrical factors than our previous instruments (von Rosenvinge *et al.*, 1969). The total collection factor at energies <1.5 GeV/nuc in the 1970 flights was ~ 3000 m^2 ster s as compared with about 600 m^2 ster s for all of our previous flights. In spite of this increase in size, the charge resolution and background suppression were considerably improved. This was accomplished by a number of new techniques: (1) The use of curved scintillators and improved compensation techniques (von Rosenvinge and Webber, 1968), which have reduced the non-uniformities due to path length and location differences in particle trajectories to $\lesssim 3\%$, a very simple expedient which provides charge resolutions which range from ~ 0.1 charge unit for Carbon to ~ 0.25 of a charge unit for Fe – at least as good as much more complex systems using spark chambers to determine the particle trajectory. (2) The use of multi-element, redundancy analysis to eliminate the effects of nuclear interactions. As the intrinsic resolution improves, point (2) becomes more important.

The net effect of these improvements is, in effect, to provide a completely new generation of instruments for studying heavy primary cosmic rays – in spite of considerable superficial similarity with past detectors.

One of the counters used was a double dE/dx-Energy-Range telescope which provided charge and isotope separation from $\sim$100–650 MeV/nuc, the energy interval depending on the charge. The other instrument was a double dE/dx-Cerenkov-Range telescope which provided detailed energy spectra over the entire energy range from $\sim$100 MeV/nuc to 1.5 GeV/nuc, but in the 1970 version did not provide isotope separation. These instruments and their charge separation and resolution capabilities are discussed in detail in a separate paper (Webber and Kish, 1971).

3. Instrument A – dE/dx × Total Energy × Range Telescope

This instrument is shown in Figure 1. It has a geometrical factor of 230 st cm^2. All four telescope elements are pulse height analyzed using separate 2048 channel analyzers. The usual mode of analysis here is the non-penetrating mode* in which

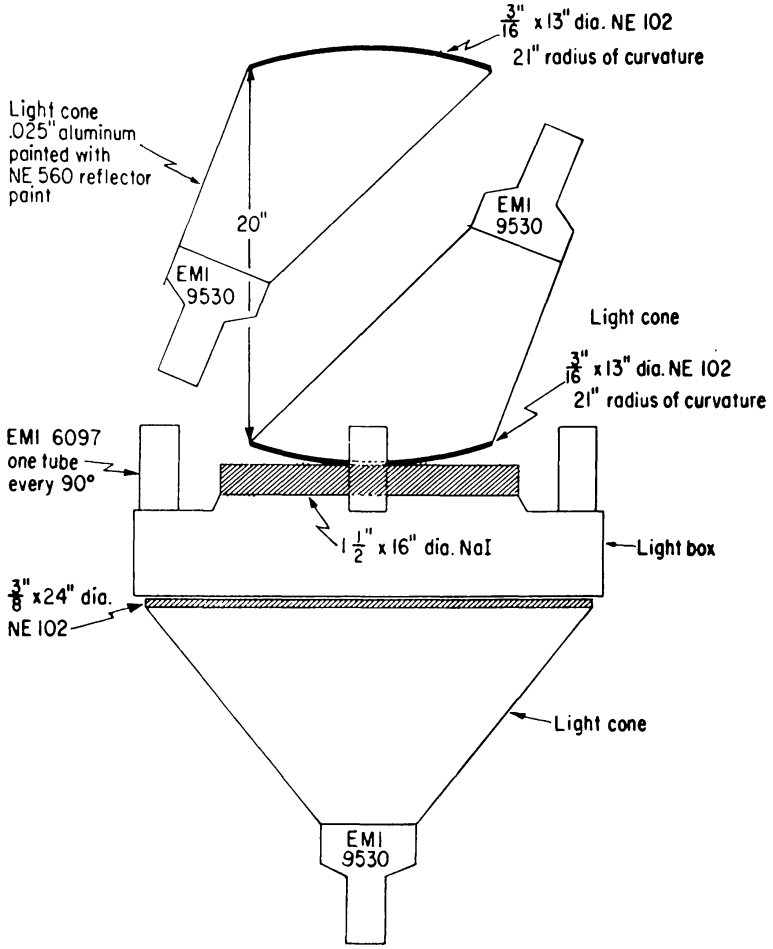

Fig. 1. Outline drawing of dE/dx·E·Range Telescope (Instrument A).

* See later discussion, however, for modifications of these criteria due to nuclear interactions.

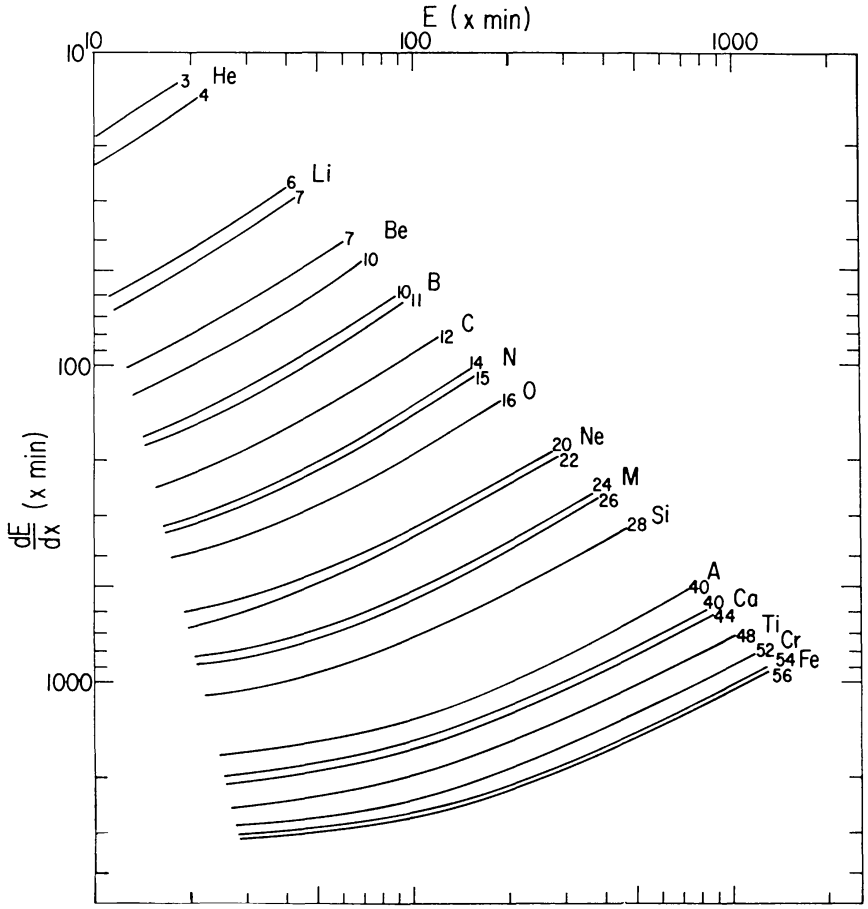

Fig. 2. Theoretical response of $dE/dx \cdot E$ Range Telescope as a function of particle charge and isotope.

a matrix is formed containing an average of the scintillation outputs of the first two curved elements (when their pulse heights lie within $\pm 12\%$ of one another) vs. the third or total energy element. The 'selection' criteria used on elements 1 and 2 greatly reduces background due to nuclear interactions and other unwanted events. The use of curved detectors reduces the contribution due to path length differences to $<3\%$ FWHM at this element separation. A theoretical response matrix for non-interacting particles of different charge and isotope stopping in the E detector is shown in Figure 2. A two-dimensional matrix of data for charges with $Z \leqslant 14$ from the 1970 flight is shown in Figure 3. The energy spectrum is determined from the energy loss scale as determined from the total E counter.

4. Instrument B – $dE/dx \times$ Cerenkov $\times$ Range Telescope

This instrument is shown in Figure 4. It has a geometrical factor of 600 st cm^2. Again all four telescope elements are pulse height analyzed using separate 2048 analyzers. The most useful mode of analysis over most of the energy range requires

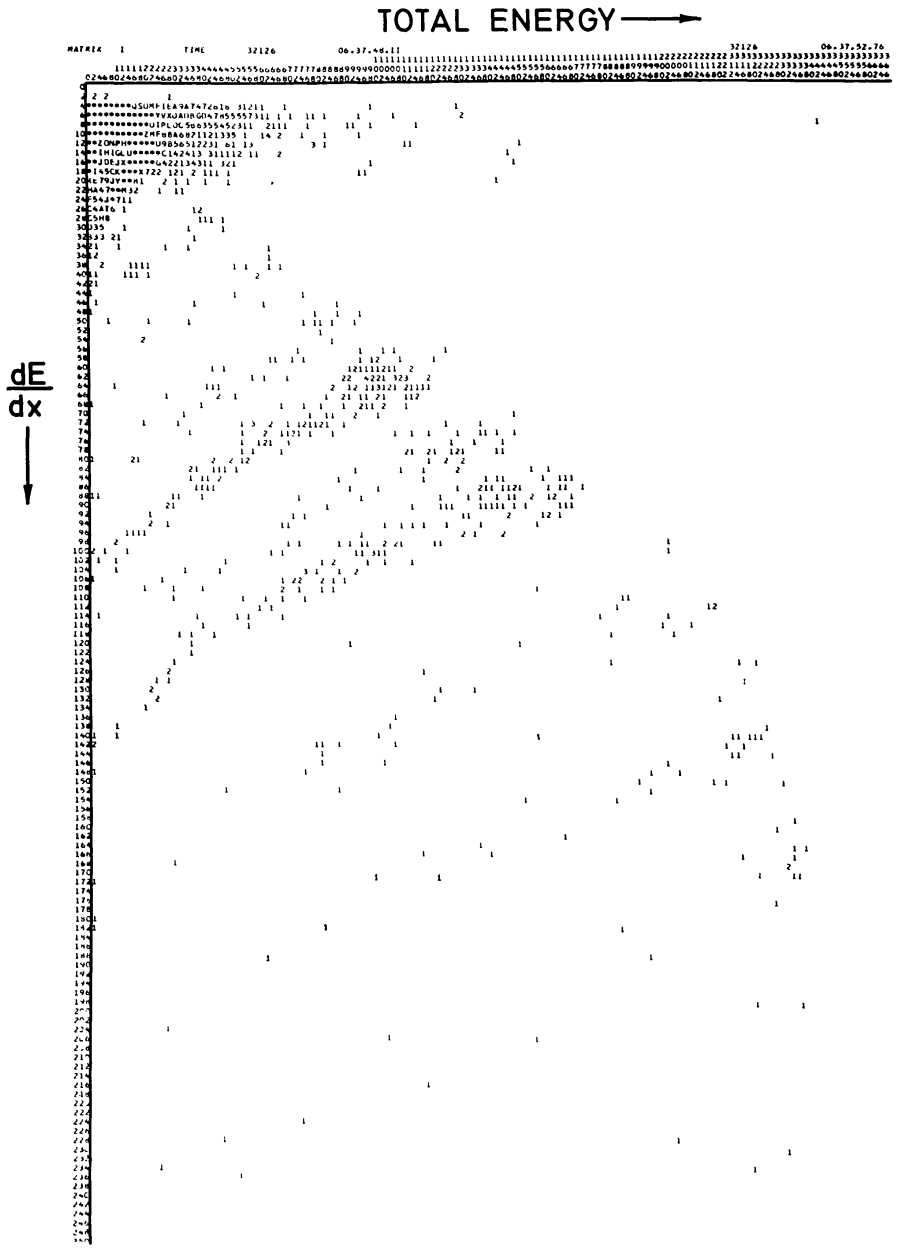

Fig. 3. Two-dimensional matrix of data from 1970 flight of Instrument A. dE/dx is increasing downwards and E increasing to the right in the figure.

that the penetration counter output be >0. In this case we form a matrix of the average of the scintillation outputs of curved elements one and two (again requiring that the pulse heights not differ by more than $\pm 12\%$) vs. the Cerenkov counter. An additional selection requirement is made for particles above the Cerenkov threshold by requiring that the normalized output of the penetration counter be within $\pm 20\%$ of the average in the first two scintillators. This two stage selection criterion reduces the 'background' between charges (mainly due to nuclear interactions in the telescope) markedly. Various combinations of selection criteria are tested to verify

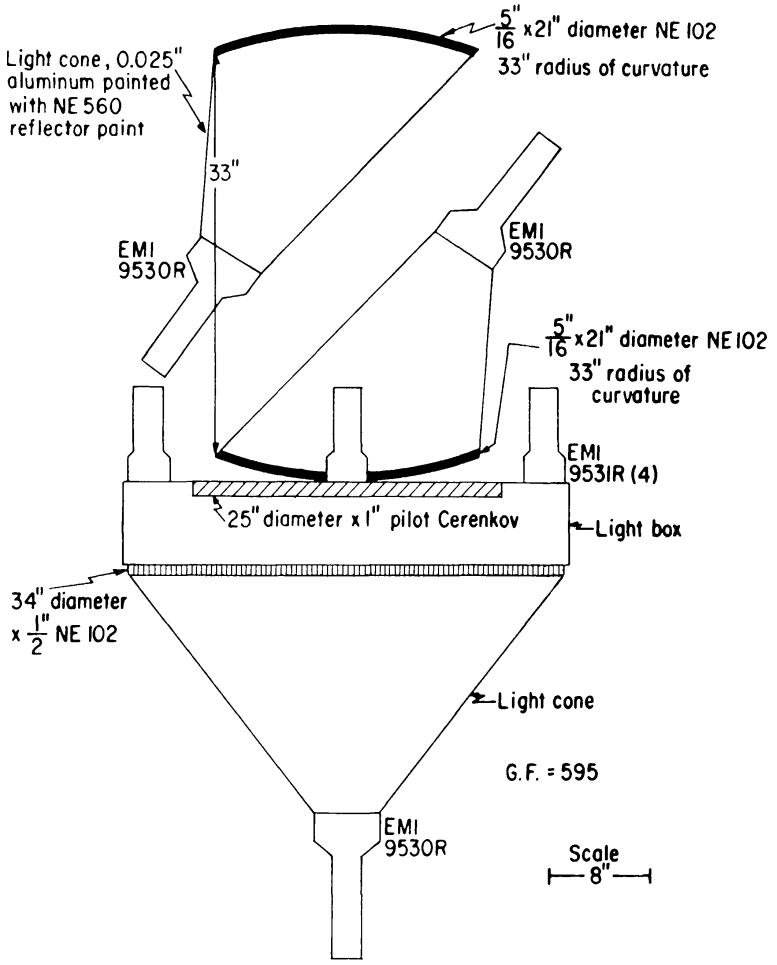

Fig. 4. Outline drawing of dE/dx·Cerenkov·Range Telescope (Instrument B).

that no non-interacting nuclei are systematically removed. The theoretical response of this telescope to particles of various charge is shown in Figure 5. A two-dimensional matrix of data for charges 2–8 from the 1970 flight is shown in Figure 6. The charge range 8-30 is shown in Figure 7. The energy scale is determined from the Cerenkov detector output only, since this output is a well-known function of charge and velocity.

The appropriate balloon flight details for the two flights are shown in Table I.

TABLE I

Balloon flight details

Date	Instrument	Altitude	Collection factor (m^2 ster sc)	Mt. Wash. neutron monitor
3 July 1970	A	2.2 g cm^{-2}	776	2063
11 July 1970	B	2.3 g cm^{-2}	2140	2107

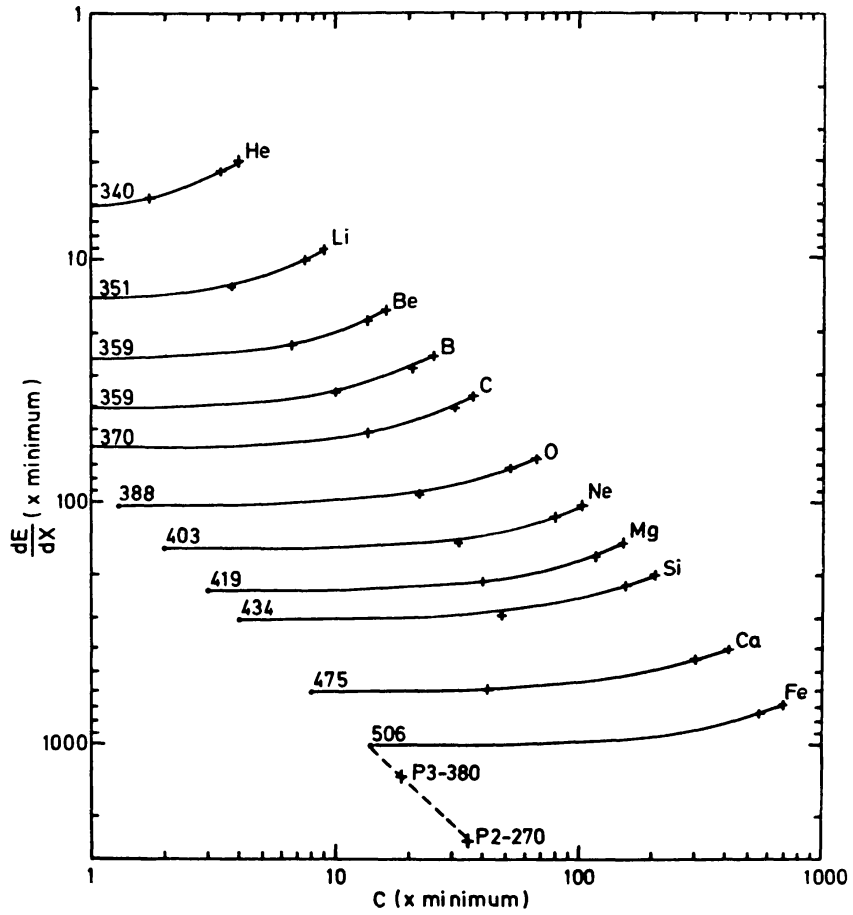

Fig. 5. Theoretical response of Instrument B to particles of different charge. The crosses and numbers refer to energies in MeV/nuc of ∞, 1000 and 500 at the top of the atmosphere. (Residual scintillation of 2 % of Cerenkov output assumed for Cerenkov detector.) Penetration limits for particles below Cerenkov threshold are shown for Fe nuclei.

5. The Raw Data

Because we are primarily interested in the relative abundances of the various charges rather than detailed energy spectra, our data analysis procedure is somewhat simplified, although by no means trivial. The most important point is to be sure that no systematic charge-dependent effects are present to distort the relative abundances, as would be determined from Figures 3, 6, and 7. Such effects would not be important in comparing adjacent charges (e.g. Mn and Fe), but could become appreciable when attempts are made to compare the relative abundance of C and Fe, for example. Such distortions could arise in two ways: (1) A relative distortion of the energy scale of the various charges. To determine the energy (in telescope B) we use the Cerenkov effect which relates the signal, N, to the velocity, β, by

$$N = Z^2(1 - 1/\beta^2 n^2) \quad n \text{ is the index of refraction.}$$

We are able to verify this relationship to within $\sim 2\%$ for relativistic particles of

Z between 2–26. Studies of non-relativistic multiply-charged particles also indicate that this formula holds to a sufficiently high degree of accuracy. Therefore, any systematic uncertainty in the energy spectra of the various charge arising from this effect would be related to the ability to accurately determine the pulse height for $\beta = 1$ particles of each charge. We estimate that this point can be located to an accuracy

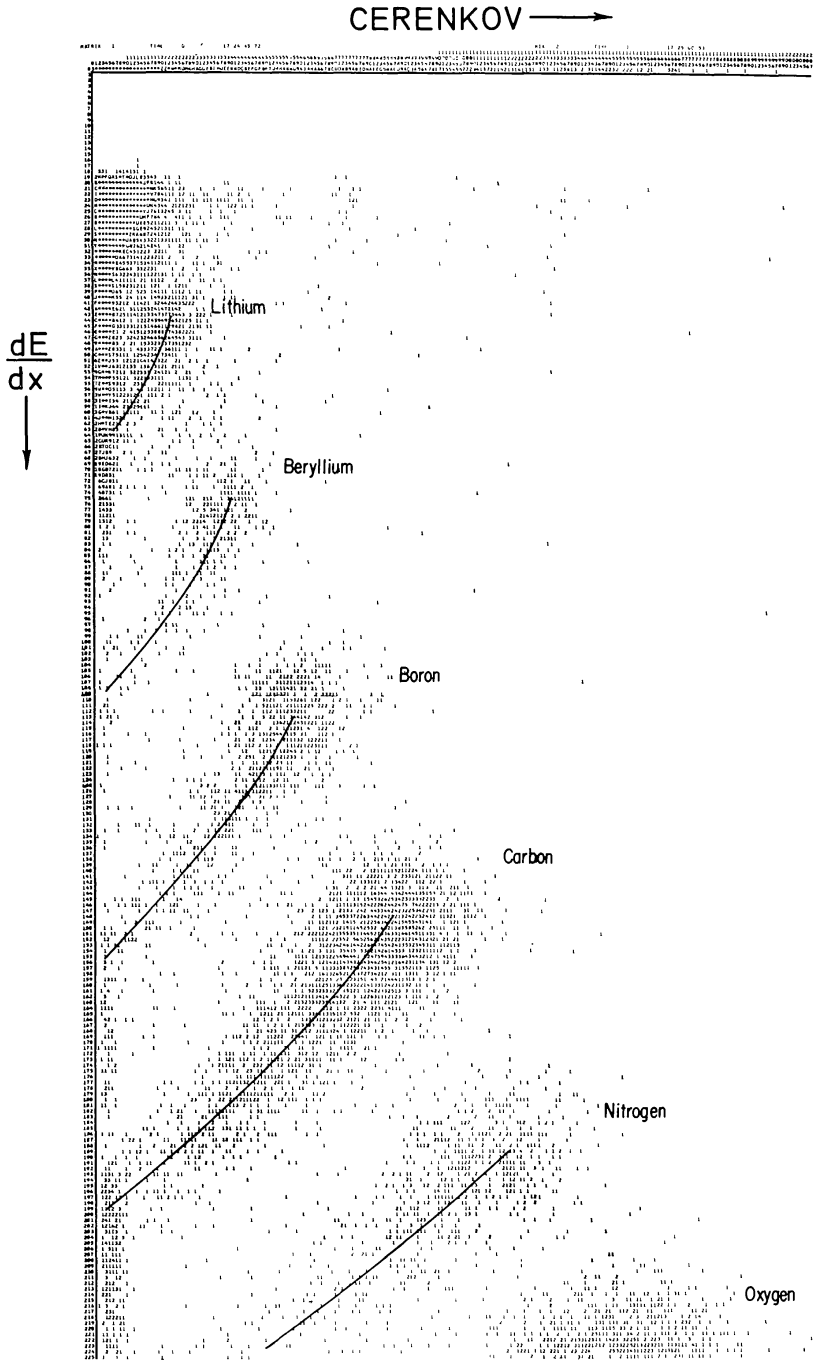

Fig. 6. Two-dimensional matrix of data from 1970 flight of Instrument B for charges 2–8. dE/dx is increasing downwards, Cerenkov output increasing to the right in the figure.

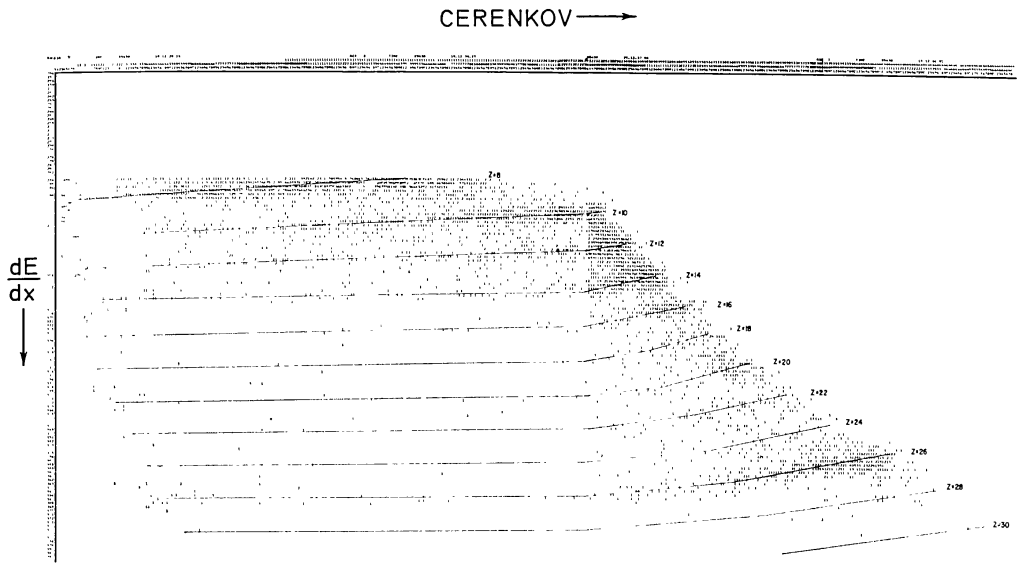

Fig. 7. Same as Figure 6 except charge range 8–30.

of $\pm 2\%$ for all charges as abundant as $0.3 \times$ Fe. At the energy of 850 MeV/nuc, the dividing energy used in this paper, the error due to this uncertainty is approximately ± 20 MeV/nuc and is negligible. (2) A possibly more serious source of distortion in the relative charge abundance is related to the 'selection' criteria that are used. The procedure of removing 'back-ground' from charge distributions using redundant measurements and requiring consistency between all measurements of a given parameter, is finding increasing use in multi-element instruments that are being used to study primary cosmic rays. If these instruments were massless, this technique would not be necessary, since the selection and consistency requirements are used to remove those events caused by particles that interact in the material of the telescope and therefore have pulse heights in one or more detectors which do not lie in a position in the two-dimensional matrix expected for a non-interacting particles.

We have utilized various combinations of selection criteria and widths of selection intervals varying from $\pm 25\%$ to $\pm 5\%$. Charge histograms (e.g. Figures 8 and 9) are

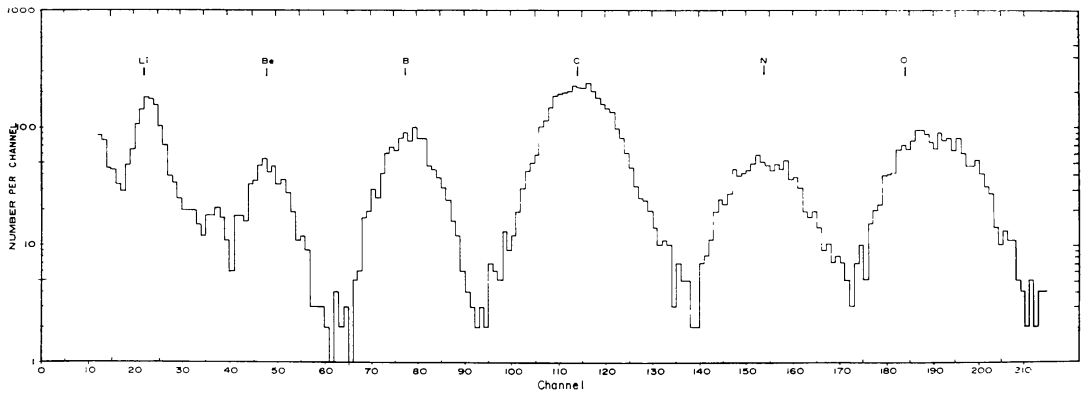

Fig. 8. Charge histogram from 1970 flight of Telescope B in Range $Z = 3$–8.

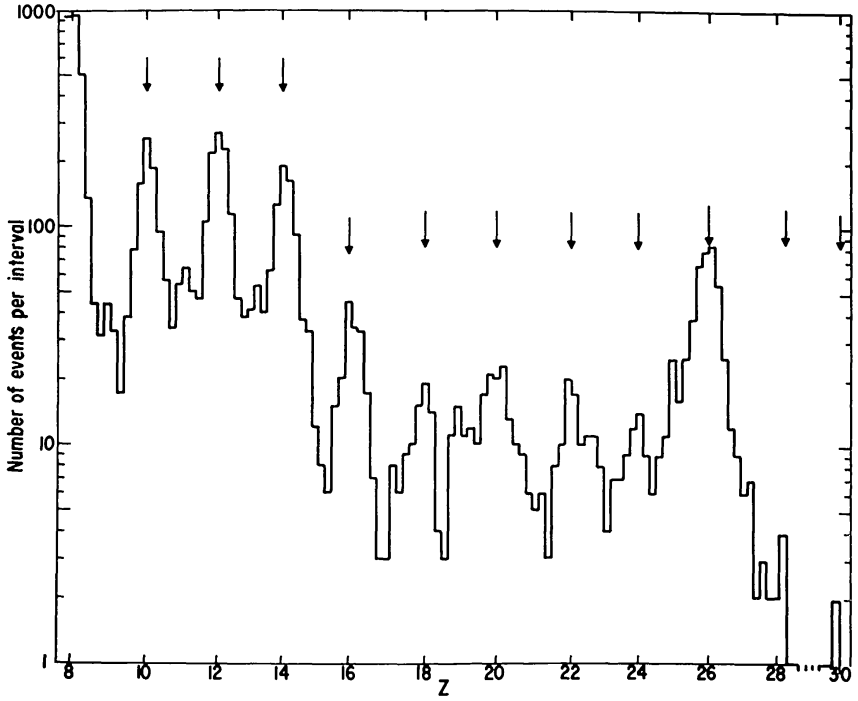

Fig. 9. Charge histogram from 1970 flight of Instrument B in charge range 8–30. Arrows show expected location of even charges.

constructed in each case and the total number of events determined for each charge. We find that the background between charges is a minimum – consistent with no removal of events from the peak of the charge distributions – for limits of $\pm 12\%$ on elements 1 and 2. By then comparing one dimensional pulse height distributions selected from the two-dimensional matrices according to the mean pulse height in elements 1 and 2 (for both telescopes A and B), we are able to determine the number of 'background' events caused by the more abundant even charges up to a $Z=14$ and by Fe that are actually removed by the selection criterion. This fraction of events is then compared with the number of particles of each of these charges that would be expected to interact, given the thickness of material in the telescope and the interaction mean free path. Within experimental error the two sets of numbers agree indicating that the selection criteria are $\gtrsim 80\%$ efficient in removing interactions occurring in the telescope.

As an example of the type of events this technique removes, we may consider Figure 7 and note the Fe nuclei that interact after the 1st two (thin) dE/dx elements can give an anomolous pulse. In the Cerenkov counter, this pulse always appears to be smaller than would have been expected from the incident particle, thus these events populate the positions to be expected for particles with $Z=22$–25. Even though a relatively small fraction of Fe nuclei interact, the abundance of Fe is so much greater than the abundance of nuclei with $Z=22$–25, that this effect is appreciable. Indeed we find the apparent intensity of $Z=22$–25 particles is reduced by $\sim 40\%$ by the application of the selection criteria. Similar effects are noted for other less

abundant nuclei located in the 'shadow' of more abundant nuclei – e.g. L nuclei (Li, Be, B) are a case in point. The energy spectra of these less abundant nuclei are distorted if this interaction background is not removed.

A different situation occurs in the total energy telescope. Here it appears that the pulse of an interacting particle in the total energy element may be larger or smaller than that to be expected for the incident particle. Thus the effect noted above is present, but to a smaller degree. In addition, a much more serious effect appears to occur. Those events of a particular charge that are 'observed' to interact, according to our selection criteria, frequently go on and produce a pulse in the penetration counter even though the energy of the incident particle is such that it would be expected to stop in the penetration counter. The fraction of this type of events increases with increasing energy and is almost 100% at energies just below the maximum energy of particles that can just stop in the total energy detector. This effect is more important for higher Z particles because of their shorter interaction mean free path and as a result can distort both charge composition results and energy spectra determined from $\mathrm{d}E/\mathrm{d}x \cdot E$ telescopes if not properly accounted for.

TABLE II

Events observed at balloon altitude

Telescope A			Telescope B	
Variable energy interval			> 850 MeV/nuc	250–850 MeV/nuc
3	64	(3.10)[a]	787	323
4	45	(2.30)	440	180
5	149	(2.05)	1392	596
6	534	(1.73)	4747	2147
7	152	(1.60)	1248	550
8	570	(1.41)	4055	1943
9	8		55	21
10	101	(1.24)	688	395
11	33		117	72
12	148	(1.13)	817	410
13	36		101	56
14	98	(1.00)	540	258
15	9		18	9
16	15	(0.91)	129	66
17	4		21	9
18	12	(0.85)	51	21
19	4		45	20
20	30	(0.75)	100	49
21	5		16	10
22	14	(0.69)	59	35
23	2		23	13
24	30		42	28
25	133	(0.63)	32	19
26			372	158
27			12	2
28	6	(0.59)	14	3

[a] Factor to normalize to constant energy interval 180–460 MeV/nuc

When we determine and compare energy spectra and absolute intensities of various charges using the two different telescopes, we obtain excellent agreement, but only after the effects of nuclear interactions are recognized and corrected for as indicated above.

Since the data presented in Figures 3, 6 and 7 represents the data after selection criteria have been imposed, we believe it to represent a measure of the correct undistorted charge composition. If we now divide this data into energy regions >850 MeV/nuc and 250–850 MeV/nuc and make cuts along lines parallel to the charge lines defined in Figure 5, we obtain the charge histograms shown in Figures 8 and 9 (Telescope B). This data, along with similar data from Telescope A but lying totally within the low energy band, constitute the basic raw data of this experiment. If we sum the data from these histograms, we obtain the individual chemical abundances at the balloon altitude. The data from telescopes A and B are summarized separately in Table II.

6. Corrections to the Raw Data

Before we can use the above chemical abundance values to study the propagation of cosmic rays in the galaxy and to determine the cosmic ray source abundances, we must make corrections for fragmentation in the residual atmosphere and for any effects of the solar modulation which might also distort the charge spectrum. The atmospheric correction is straightforward and is minimized because of the small atmospheric depths at which the instruments floated. A very crude estimate of its importance relative to an equivalent amount of interstellar material may be made by simply comparing the interaction mean free paths in air and hydrogen. The ratio $\lambda_{\text{air}}/\lambda_{\text{H}}$ is typically ~ 5 for charges between 6 and 26, so that the 2.3 g cm^{-2} of residual atmosphere is equivalent to roughly 0.5 g cm^{-2} of interstellar material, (assuming equal fragmentation parameters in air and hydrogen). Since we observe that the heavy cosmic rays appear to have travelled through $\sim$2–3 g cm^{-2} of interstellar hydrogen, this correction is not negligible and in fact for depths $>$4–5 g cm^{-2} becomes very important.

A complete treatment of this problem requires a knowledge of all the relevant interaction (fragmentation) parameters in air. Unfortunately these are even less well known, on an individual basis, than those in hydrogen.

We have used the concept of the absorption length, $\Lambda_i = \lambda_i/(1-\sum_j P_{ij} N_j/N_i)$ where λ_i = interaction MFP, P_{ij} are the fragmentation parameters for the production of the ith component from the jth heavier components and N_i, N_j the abundances of the various nuclear species; to extrapolate the individual charge abundances through air to the top of the atmosphere and have derived a set of Λ_i using estimates of individual and collective fragmentation parameters in air as given by von Rosenvinge (1969) and by Cleghorn (1969). The values of Λ used are listed in Table III. In some cases the values of $\Lambda_{\text{air}} \to \infty$ (and could actually be negative) indicating that the secondary atmospheric production is actually as great or greater than the attenuation of those 'primary' particles incident on the top of the atmosphere.

TABLE III

Interaction MFP and correction factors for 2.2 g cm^{-2} of Air

Charge	Air			Hydrogen
	λ(g cm^{-2})	A(g cm^{-2})	Factor	λ(g cm^{-2})
3		–	1.01	11.3
4		–	1.01	10.0
5		–	1.01	8.8
6	28.2	33.0	1.071	7.9
7	27.0	36.0	1.063	7.0
8	25.9	30.0	1.078	6.2
9		–	~ 1.00	
10	23.8	32.0	1.073	5.2
11	22.9	42.0	1.04	
12	22.0	26.5	1.088	4.4
13	21.4	32.0	1.073	
14	20.7	22.0	1.110	3.9
15		–	~ 1.00	
16	19.6	24.1	1.100	3.55
17		–	~ 1.00	
18	18.6	27.6	1.087	3.30
19		–	~ 1.00	
20	17.6	22.1	1.110	3.09
21		–	~ 1.00	
22	16.6	–	~ 1.02	2.83
23		–	~ 1.00	
24	15.6	29.0	1.08	2.60
25		–	~ 1.02	
26	14.5	14.5	1.165	2.45
27		–	–	
28	14.0	14.0	1.171	2.35

The correction of the relative charge abundances for solar modulation is probably not serious, but unfortunately is not well known. The fact that our measurements were made in 1970 when the solar modulation was near its maximum will, of course, tend to amplify these effects. The usual argument is made that the solar modulation will not change the ratios of any two charges with identical mass to charge ratios if their interstellar spectra are identical. There is no evidence contrary to the above statement, and in addition the differences between spectra of the various charges appear to be small so that the principal effects of solar modulation would be expected to occur on particles with different mass to charge ratios. These effects will depend on the detailed rigidity dependence of the modulation but are expected to be small in any case (see e.g. discussion by von Rosenvinge *et al.*, 1969). As a result, we shall not make any corrections on the abundance ratios for solar modulation.

The following important point should be kept in mind regarding the effects of solar modulation and interplanetary energy loss, however. A number of studies (Goldstein *et al.*, 1970; Lezniak and Webber, 1971) have indicated an effective average energy loss ~150 MV occurring in interplanetary space even at times of minimum modulation. Recent work (Lezniak and Webber, to be published) indicates that the

average energy loss is ~600 MV in 1970. This energy loss is expected theoretically from betatron deceleration in the expanding solar wind (Gleason and Axford, 1968; Jokipii and Parker, 1970) and for nuclei with $A/Z=2$ corresponds to an average energy loss ~300 MeV/nuc in 1970. The energy interval 250–850 MeV/nuc corresponds therefore to ~550–1150 MeV/nuc in interstellar space.

This interplanetary energy loss probably means that we cannot observe directly the interstellar cosmic ray abundances at the lowest energies. On the other hand, since energies ~300 MeV/nuc at earth correspond to ~600 MeV/nuc in interstellar space, interstellar ionization loss effects are relatively unimportant even for 300 MeV/nuc particles at earth.

7. The Results

The relative abundances of all charges at the top of the atmosphere (normalized to 0=1000) are shown in Table IV for the two energy intervals discussed earlier. This data form the basis for the further discussions in this paper. Figure 10 shows the abundances observed at high energies in this experiment as compared with other earlier experiments. We note the following points from Table IV: (1) Generally

TABLE IV

Relative abundances of cosmic rays at Earth, 1970

Charge	> 850 MeV/nuc	Pioneer > 1100 MeV/nuc		250–850 MeV/nuc
3	167 ± 7	158 ± 8	(465)	177 ± 9
4	97 ± 5	80 ± 6	(235)	88 ± 6
5	305 ± 9	270 ± 9	(1015)	296 ± 11
6	1140 ± 20	1111 ± 23	(3275)	1082 ± 23
7	275 ± 9	288 ± 9	(855)	278 ± 12
8	1000	1000	(2950)	1000
9	13 ± 2	18 ± 3	(52)	12 ± 26
10	178 ± 7	189 ± 8	(557)	191 ± 9
11	29 ± 3	38 ± 4	(110)	38 ± 4
12	206 ± 7	194 ± 8	(575)	200 ± 9
13	26 ± 3	42 ± 4	(124)	34 ± 4
14	136 ± 6	145 ± 7	(415)	134 ± 7
15	4.5 ± 1.1			6 ± 1.5
16	35 ± 3			28 ± 3
17	5.6 ± 1.2			4.2 ± 1.2
18	13 ± 2			13 ± 2.2
19	12 ± 2			9 ± 1.8
20	26 ± 2.5			29 ± 3
21	4 ± 1.1			5.6 ± 1.5
22	14 ± 2			19 ± 2.6
23	5 ± 1.2			7 ± 1.5
24	10.7 ± 1.8			20 ± 2.7
25	8.5 ± 1.6			12 ± 2.2
26	105 ± 5			99 ± 6
27	3.9 ± 1.0			1.6 ± 0.8
28	4.4 ± 1.1			2.9 ± 1.1

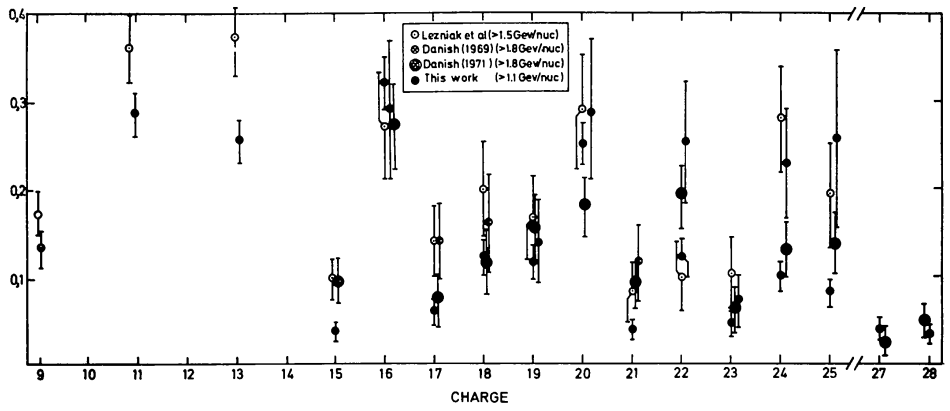

Fig. 10. Relative abundance of various nuclei relative to Fe at the top of the atmosphere for energies > 850 MeV/nuc. Other recent experimental results are also shown (Danish 1969 = Dayton *et al.*, 1970; Danish 1971 = Casse *et al.*, 1971).

there are no significiant differences in chemical abundance between the two energy intervals considered here. Possible exceptions to this statement occur for Cr and Mn, where the higher abundances at lower energies may be related to the increased fragmentation cross section of these nuclei from Fe; and for Na and Al, where we observe apparently significant differences in the high and low energy abundances. As a result we also show data for these nuclei from the Pioneer 8 satellite for an equivalent high energy interval (Lezniak *et al.*, 1970). The abundances of Na and Al observed on Pioneer 8 at high energy agree with those presented here at low energy, and we must believe that the lower abundances found in this paper at high energy represent extreme statistical fluctuations ($\sim 3\sigma$) or unknown systematic effects.

Some important differences exist between the abundances we measure and earlier work as summarized in the review of SS. The most important and obvious of these include: (1) The O/Fe ratio which is 9.6 ± 0.4 in this study and 7.6 ± 0.9 according to SS. (2) The Cr/Fe ratio which is 0.10 ± 0.02 in this study and 0.31 ± 0.09 according to SS. Other detailed differences exist, and we should also note that we observe a relatively low Mn abundance at lower energies, in contrast to some earlier results (Price *et al.*, 1970; Waddington *et al.*, 1970), but in better agreement with others (Garcia-Munoz and Simpson, 1970).

8. The Interstellar Propagation

The cosmic ray abundances summarized in Table IV contain both particles which have been directly produced in the cosmic ray sources (primaries), as well as particles produced by interactions of these primary particles with interstellar hydrogen enroute to the earth (secondaries). An accurate determination of the fraction of each type of secondary particle produced depends on a knowledge of the relevant fragmentation parameters and on the models assumed for the interstellar propagation.

As the composition data at Earth has become more accurate, more elaborate assumptions must be made regarding the propagation. Two simple extremes for the

interstellar propagation may be considered: a slab matter length, X_s, wherein all particles (of all energy) are assumed to have travelled through the same amount of matter – roughly equivalent to propagation down a pipe – and an exponential distribution of matter path lengths $N(X) \sim \exp(-X/X_e)$ where X_e is a characteristic matter length, in effect the 'leakage length' (or age since $X_e = \beta c \varrho T_e$). This is the 'steady state' picture as developed by Cowsik, *et al.*, (1967). This path length distribution is roughly equivalent to that obtained for a point source of cosmic rays diffusing into an infinite medium under steady state conditions.

A principal requirement of any model is that the source abundance $\to 0$ for all obvious 'secondary' nuclei for a given matter length parameter X_s or X_e. Previous work has indicated that a single value of X_s (e.g. 4 g cm^{-2} of hydrogen) which is sufficient to make the source abundance of L nuclei $\to 0$ will produce too many secondaries from Fe (Waddington *et al.*, 1970; Lezniak *et al.*, 1970). However, a single value of the 'leakage length' $X_e \sim 5$ g cm^{-2} will effectively explain the observed 'secondary' abundances produced by all primary charges with Z between 2 and 26. Because of the improved accuracy of our data, we would like to take this argument one step further and examine whether it is possible to distinguish, using available chemical composition data, between an exponential path length distribution and other path length distributions which may represent the cosmic ray propagation – source distribution. Fichtel and Reames (1968) have discussed a number of such possibilities which result in matter length distributions which differ slightly from the exponential. More recently Lingenfelter *et al.* (1971), Ramaty and Lingenfelter (1971) and Pacheco (1971) have discussed the propagation problem for a wide variety of diffusion and boundary conditions. Some of the resulting path length distributions obtained differ considerably from a simple exponential.

In order to examine this problem in a useful way, we must derive a way of presenting the data for a given model that will illustrate how well a given fixed set of parameters for that model fits the data on fragmentation for all charges. To do this we develope the concept of an 'equivalent' slab length as follows: One can show that for the slab length model, the production of secondaries of charge Z from a primary of charge $Z+1$ is given by

$$j_i \sim P_{ki} X_s \tag{1}$$

where X_s is the amount of material traversed and P_{ki} is the fragmentation probability for the production of an ith nucleus in the interaction of a kth (primary) nucleus with interstellar hydrogen. Here it is assumed that the interaction MFP for the ith and kth nuclei are identical (a close approximation for nearly adjacent charges) and that interstellar ionization energy loss can be neglected. We have carried out exact calculations which show that above ~ 500 MeV/nuc the neglect of ionization energy loss introduces a negligible error for the matter path lengths we are considering. Since we believe that because of interplanetary energy loss, our lower limit of 250 MeV/nuc corresponds to at least 500 MeV/nuc in interstellar space, the ionization energy loss effects can be neglected for both of our energy ranges.

Similarly, if we neglect ionization energy loss, we have for the secondary production in the case of an exponential distribution of path lengths

$$j_i \sim P_{ki}\left(\frac{1}{\lambda_i}+\frac{1}{X_e}\right)^{-1} \tag{2}$$

where λ_i = interaction MFP, and X_e = 'leakage' length. By comparing the above equations we may define an 'equivalent' slab length X

$$X \sim \left(\frac{1}{\lambda_i}+\frac{1}{X_e}\right)^{-1} \tag{3}$$

which will give the same production of different secondary charges as an exponential path length distribution with escape length X_e in g cm^{-2}. Note that this value of X will be dependent on charge. Indeed if we choose X_e to be 5 g cm^{-2}, then X varies

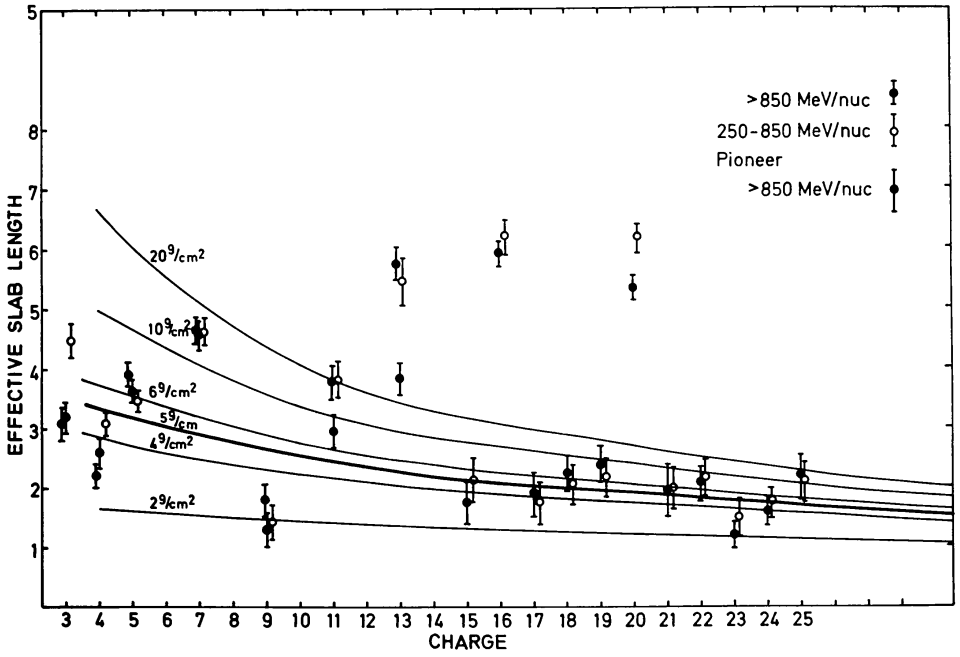

Fig. 11. Effective slab length as a function of charge. Experimental points show the amount of interstellar material required to produce the observed charge abundances in the slab length approximation. Lines show the equivalent slab length for exponential path length distributions with different leakage lengths X_e.

from $\sim$2 g cm^{-2} for nuclei just below Fe in the periodic table to $\sim$4 g cm^{-2} for Li, Be, and B which are produced mainly by C and O. The quantitative details of an *exact* calculation for both types of path length distribution are shown in Figure 11. This calculation makes use of the fragmentation parameters for Fe given by SS at high energies and those given by Waddington (1969) for other charges (adjusted to agree with the SS estimates for Fe $\rightarrow$ Al, K, Ca, and Mn) at 700 MeV/nuc for the 250–850 MeV/nuc energy interval. The 'equivalent' amount of interstellar hydrogen

required to produce the *observed* abundances of various secondary nuclei is also shown in this figure. The variation of the 'equivalent' path length for various values of the leakage length is also illustrated in this figure. The actual values for the various charges are from exact calculations which confirm the accuracy of the approximate relation (3).

We believe that this representation brings into focus some of the differences between the path length distribution models in terms of their effects on the observed 'secondary' charge distribution more clearly. We observe, for example, that if a slab length is the correct path length distribution, then the observed abundances of secondary nuclei would all be produced by an effective slab length which is independent of charge. The abundance of certain nuclei, such as N, Na, Al, S, and Ca clearly do not fit this picture, or any other simple picture for that matter, and must therefore be regarded as being present in the source in appreciable numbers. All of the remaining nuclei shown on the graph qualify as 'secondary' nuclei. All of these nuclei with $Z \geqslant 9$ could indeed be produced by an effective slab length ~ 2 g cm^{-2}, however when one includes Li, Be, B, then the charge dependence of the effective path length becomes important and the data fits better the exponential model with $X_e = 5 \pm$ ± 1 g cm^{-2}. There is a considerable scatter about the 5 g cm^{-2} line, however, due in part to uncertainties in the fragmentation parameters, and in part to uncertainties in the composition data. This scatter of points limits our ability to use chemical composition data to deduce the correct interstellar path length distribution. To see this point more clearly, we shall consider several other path length distributions and represent them in terms of an 'effective' slab length vs. charge, as we have done for an exponential distribution. The other types of path length distribution we consider are: (1) An exponential distribution cutoff at 0.5 g cm^{-2} as used by SS. (2) A model discussed by Fichtel and Reames (1968) in which the path length distribution arises from a uniform spherical distribution of sources with the Sun at its center. Cosmic rays then diffuse throughout this region with the scale of the path length distribution, $P(X)$, being determined by the quantity R_0^2/λ where $R_0 =$ radius of region, $\lambda =$ MFP for diffusion. The value used by Fichtel and Reames was $R_0^2/\lambda = 9.3$ g cm^{-2}, constant with energy. The two other models are extreme cases discussed by Ramaty and Lingenfelter (1971). In (3), a uniform flat disk shaped source distribution with thickness in the Z dimension, $b \sim 100$ pc and approximately equal to the scale height of interstellar hydrogen perpendicular to the galactic plane is used. It is assumed that the Sun is located in the galactic plane ($Z = 0$). Isotropic diffusion is assumed to take place in a similar disk-shaped region of thickness $a = 2b$ with a reflecting boundary. In (4), the situation is identical to (3) except $a = 3b$ and the boundary is assumed to be absorbing. Path length distributions for models (3) and (4) have more long path lengths than the exponential distribution. This is a result of the geometry used in which the thickness of the trapping volume is larger than that of the source, so that particles produced close to the plane can re-enter the central parts of the disk after a relatively long trapping time in the confinement volume. This might be representative of a disk-halo configuration, for example.

The vacuum path length distributions for these models are shown in Figure 12. We note that a source distribution similar to (3) or (4), but with diffusion into an infinite medium, as well as the compound diffusion model of Lingenfelter *et al.* (1971), produce vacuum path length distributions which are intermediate between models (3) and (4).

A comparison of previous calculations of secondary production using these models

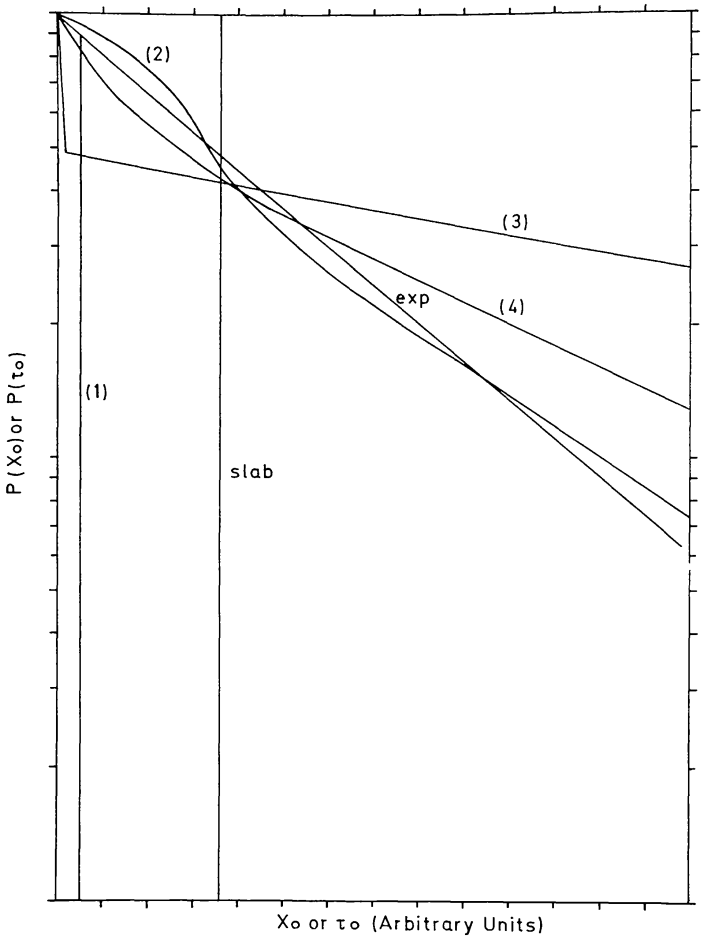

Fig. 12. Vacuum path length distributions for various propagation models as discussed in the text. (1) Exponential distribution, cutoff at 0.5 g cm^{-2}; (2) Model used by Fichtel and Reames (1968); (3) Reflecting Boundary model and (4) Absorbing Boundary model (Ramaty and Lingenfelter, 1971).

has been complicated by the fact that different sets of fragmentation parameters and source abundances were used by different authors. Our calculations make use of the same set of fragmentation parameters (as noted above) and source abundances for each model.

The effective slab length as a function of charge that we obtain for each of these models (normalized to that for $Z=6$ particles as obtained for the exponential distribution with $X_e=5$ g cm^{-2}) is shown in Figure 13. We also show the normalized

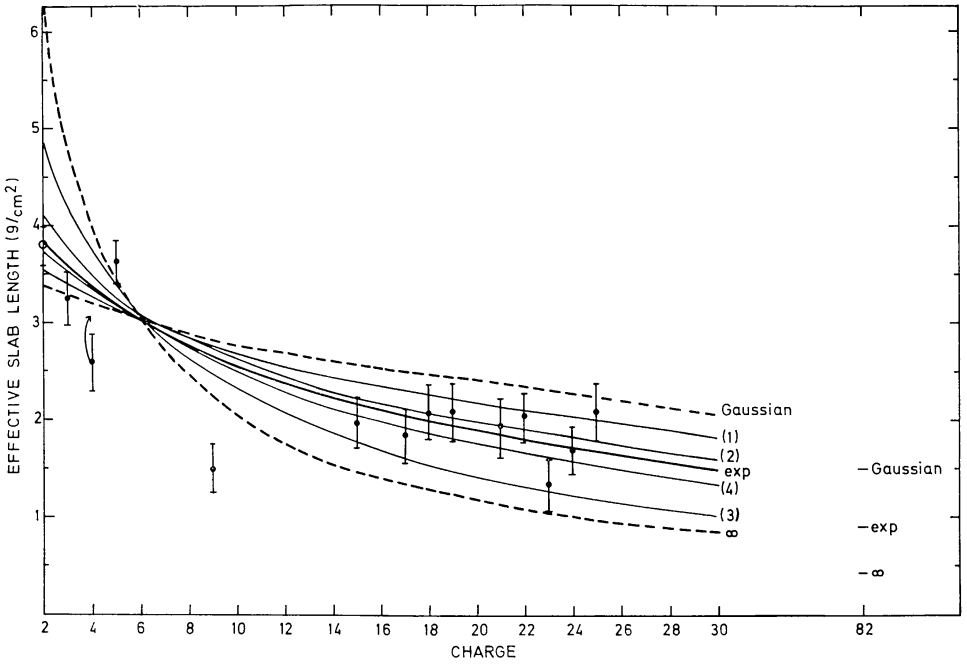

Fig. 13. Effective slab length as a function of charge for various propagation models. Numbers refer to models listed in caption for Figure 12. Other models are discussed in text.

effective slab length that would be obtained for the limiting case of an exponential distribution with $X_e \to \infty$ and for a Gaussian path length distribution centered at $4\ \mathrm{g\ cm^{-2}}$. We believe that these two latter distributions represent the possible extremes to be expected on almost any galactic cosmic ray propagation model. We observe that a path length distribution extending to large values of X will tend to produce relatively less fragmentation products of the iron or heavier groups for the same L/M ratio as the exponential distribution with $X_e = 5\ \mathrm{g\ cm^{-2}}$, e.g. models (3) and (4) or the exponential model with $X_e \to \infty$. Conversely, models which are relatively deficient in short path lengths will tend to produce a smaller variation in effective slab length as a function of charge – gradually approaching that for a simple slab length.

For the data points in this figure, we have shown only the obvious secondary nuclei and have taken an average of the high and low energy data shown in Figure 11. If we ignore the data point for F, for which the fragmentation cross sections that have been used must obviously be in error, and also accept the fact that most of the Be^{10} has decayed, thus raising this point according to the arrow in Figure 13, then the observed charge dependence of the effective path length seems to rule out the two extreme possibilities considered above as well as most likely models (1) and (3). The other models discussed above, including the compound diffusion picture, would fit the data, however.

It should be pointed out that measurements at both high and low charge are particularly valuable for determining the correct path length distribution. Measure-

ments of the fragmentation of Pb, for example, would effectively sample the distribution at short path lengths and the fragmentation of He^4 into H^2 and He^3, the distribution at longer path lengths. In Figure 13, we show the effective slab length for the production of secondaries by Pb for the 5 g cm^{-2} exponential model and for the two extreme distributions considered earlier. In the case of secondaries from He^4 fragmentation, the He^3 intensities are quite well known (e.g. Baity *et al.*, 1971). Utilizing the latest work on the fragmentation parameters into He^3 summarized by Meyer (1971) and calculations of the effects of interplanetary modulation we have determined that the observed $He^3/(He^3+He^4)$ ratio of 0.10 at low energies is consistent with an effective slab length of 3.8 g cm^{-2} for He^3 production ($X_e=5$ g cm^2 for the exponential model). This point is also shown in Figure 13. It must be emphasized, however, that this comparison could be better carried out if He^3 measurements were available above the limit of $\sim$200 MeV/nuc available now and at a time of minimum solar modulation.

It should also be pointed out that essentially the same information on the path length distribution as is contained in the charge composition data is also contained in the low energy composition data where interstellar ionization energy loss effects are important. This Z^2 dependent energy loss manifests itself in a change in the observed abundance ratio of two charges at a given energy such that if one takes the ratio of nuclei of charge Z to $Z+1$, this ratio will increase as one goes to lower energies, if it is assumed that this ratio is constant at the source. This increase is greatest and quite large for a slab length distribution, but is much less for an exponential path length distribution. This is because the effective path length decreases at lower energies since particles with long path lengths are unable to reach the observer because of energy loss. The observational fact is that the charge ratios change only slightly at low energies even for the extreme case of the He/Fe ratio. Originally Comstock (1969) and Waddington and Freier (1968) interpreted this behavior in terms of a 'second' component of cosmic rays at low energies that had undergone very little fragmentation. Von Rosenvinge *et al.*, (1969), using more extensive data and considering various path length distributions, concluded that the lack of change in the charge ratios at low energies was consistent with distributions of path lengths similar to the exponential one or that proposed by Fichtel and Reames (1968). Essentially similar conclusions were reached by Shapiro *et al.*, (1970).

If interplanetary energy loss plays an important role, as we have indicated earlier may be the case, it becomes questionable whether the low energy cosmic rays observed at Earth can really provide information on the spectrum in interstellar space at low enough energies so that the ionization loss effects become dominant. In any case, one has to understand the interplanetary modulation effects better, and to have new spectral measurements of the different charges at times near sunspot minimum before this approach can be fully utilized.

Finally, we should mention another very powerful approach to the same problem using radioactive secondary isotopes. At the present time the study of Be^{10} with a half-life of $\sim 3\times 10^6$ yr is the only one that is feasible. A very interesting study of

sensitivity of the Be^{10} abundance as a function of energy to various path length distributions has been carried out by Meneguzzi *et al.* (1971).

9. The Fragmentation Parameters

It is obvious from the data presented in Figures 11 and 13 that uncertainties in the fragmentation parameters play at least as important a role as uncertainties in the charge composition data in trying to determine how well the data fits a particular propagation model.

Let us consider that an exponential matter length distributions with $X_e = 5$ g cm^{-2} of hydrogen is a correct representation of the cosmic ray propagation problem. We might then assume that the scatter of points about this line in Figures 11 and 13 is due to errors in the fragmentation parameters only and in a sense reverse the problem as considered previously by now using the measured abundances to determine the correct fragmentation parameters. Let us examine this approach individually for certain 'secondary' nuclei that appear to deviate by more than 2σ (average high and low energies) from the $X_e = 5$ g cm^{-2} curve. We assume that the positive deviations of N, Na, Al, S, and Ca represent the fact that these nuclei are present in the source, and they will be discussed in the following section. This leaves the nuclei F and Mn. Mn is produced only by Fe, so the situation here is relatively simple. Previous calculations have assumed Mn^{55} and Mn^{53} are stable, but Mn^{54} is not. Furthermore, the cross section, σ, for Mn^{55} production is assumed to be the same as $\sigma(Fe^{56} \rightarrow Fe^{55})$. Casse (1971) has recently calculated that relativistic Mn^{54} will have a half-life $\sim 1.5 \times 10^6$ yr and therefore might be present in the cosmic rays, and has suggested a revised (increased) value for the Mn^{55} production cross section. If his arguments are correct and Mn^{54} is included, a value of ~ 90 mb is more correct for the total Mn cross section at high energies instead of the value of 52 mb we have used. If the 90 mb cross section is used the new effective slab length for Mn would be in slightly better agreement with the $X_e = 5$ g cm^{-2} line, however the data requires a value of 75 mb for this cross section to exactly agree with the $X_e = 5$ g cm^{-2} model. At the present level of accuracy of our data and of the fragmentation parameters then it is not possible to determine whether Mn^{54} is present or not.

In the case of F, we can only conclude that the cross sections we have used must be too high by at least 50%. Since the cross sections for F^{19} have not been directly measured but deduced from symmetric reactions, such a discrepancy would not be too surprising.

10. The Cosmic Ray Source Composition

One of the principal aims of the cosmic ray composition studies is to be able to determine the actual composition of these particles at the source. In comparing the calculations for the various propagation models as considered in the previous section, we find that the precise source composition does not depend critically on the propagation model as long as it has a path length distribution similar to that of the $X_e =$

$= 5$ g cm^{-2} exponential model. In fact, for models (2) and (4) we find that the propagation model differences in the source composition are much less than those due to the uncertainties in the fragmentation parameters or in the composition data itself.

This allows for fairly precise model independent estimates of the source composition to be made based on the particularly simple formulae of the steady state – exponential path length distribution model.

If we first take the observed abundance of all of the nuclei (relative to say Fe) at the top of the atmosphere, and then subtract the contribution of secondaries using the exponential path length distribution model with $X_e = 5$ g cm^{-2}, we obtain the residual primary intensity. Again neglecting the effects of ionization energy loss this residual primary intensity at earth is simply related to the source abundance by

$$j_{ip}(E) \sim j_{is}(E)\left(\frac{1}{\lambda_i} + \frac{1}{X_e}\right)^{-1}.$$

Source abundances deduced in this way are shown in Figure 14 and also in Table V. The errors shown are due to the statistical accuracy of the abundance measurements *only*.

Before making the usual comparison of these abundances with solar or cosmic

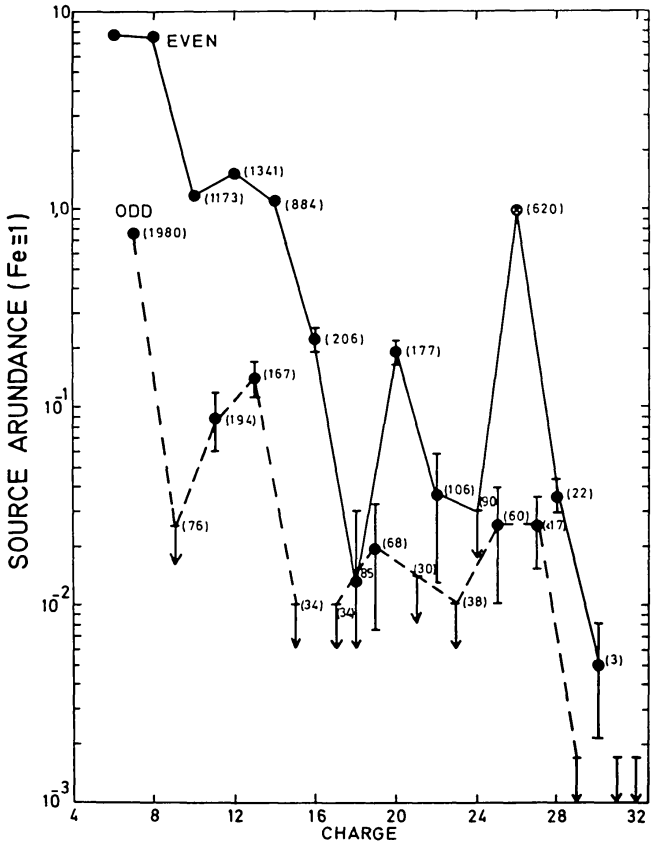

Fig. 14. Cosmic ray composition at source as deduced from measurements at Earth and using an exponential path length distribution model with $X_e = 5$ g cm^{-2}.

TABLE V

Cosmic ray source abundances (Fe = 1000)

Charge	Cosmic ray source	Meteoritic[a]	Solar[b]	Ratio $\left\{\frac{\text{Cosmic ray source}}{\text{meteorite}}\right\}$
6	5150	15200	11000	0.34
7	565 ± 80[c]	2740	2400	0.21
8	5470	26500	21500	0.21
9	< 25	4.0		
10	868	2550	2400	0.34
11	67 ± 20	70.2	75	0.95 ± 0.28
12	1200	1170	880	1.01
13	110 ± 22	95.3	48	1.14 ± 0.24
14	890	1120	720	0.76
15	< 10	14.1		
16	175 ± 25	569	670	0.30 ± 0.05
17	< 10	2.2		
18	15 ± 15	128		
19	19 ± 12	3.6	1.3	
20	130 ± 20	83	18	1.6 ± 0.25
21	< 15	0.03		
22	35 ± 22	2.6	1.5	
23	< 10	1.0	0.7	
24	< 30	13.9	1.6	
25	25 ± 15	9.9	1.3	
26	1000	1000	1000	
27	< 25	2.6	1.2	
28	35 ± 7	51.5	13	0.70 ± 0.14
29	< 1.7	1.0	1.0	
30	5 ± 3	1.7	0.13	2.9 ± 1.7

[a] Cameron (1969)
[b] Unsold (1969)
[c] $\pm 10\%$ errors on fragmentation parameters

abundances, we should briefly make a comparison of our source composition data with previous work. In this connection, the standard of reference is the detailed compilation of SS. Our data considerably extends this work for nuclei of low source abundance, but in addition there are discrepancies for some of the more abundant nuclei. The most striking of these relate to the C/Fe or O/Fe ratios. We determine them to be ~ 5.2 whereas SS find ~ 4.4. This difference cannot be related to systematic effects in the charge interval between O and Fe, since this same effect is also noted in the O/Si ratio which is 6.2 in our case and 4.4 according to SS. In other words, the Si/Fe ratio, which relates to a very large interval in Z, is virtually the same in both cases. These differences arise, of course, from the basic composition differences at the top of the atmosphere as noted earlier. It should be pointed out that the SS values are above a given rigidity (4.5 GV). To compare with our values above a given energy/nucleon a multiplicative factor $\sim A/2Z$ of the respective charges must be applied. This factor is typically ~ 5–10% and will reduce these differences but not

completely eliminate them. We believe that the correct C/Fe or O/Fe ratios both at the top of the atmosphere and at the cosmic ray sources are larger than determined by SS. This has some rather interesting consequences, as will be noted later.

Other differences relate to the source abundances of Na and Al and Ca, which we can now determine quite accurately in contrast to upper limits in the study of SS and to Cr, for which we find a source abundance <0.03 of Fe in contrast to a value $\sim 0.2 \times$ Fe determined by SS. Our upper limits to the charges which are very scarce in the source are generally $\sim 0.02 \times$ Fe.

If we turn our attention now to a comparison of our cosmic ray source composition data with the meteoritic or solar abundances as listed in Table V, we immediately run up against a history of statements to the effect that the cosmic ray composition is overabundant in heavier nuclei. This is still a correct statement when the comparison of the individual heavy nuclei abundances is made with hydrogen and helium, however this statement has sometimes been taken to mean that even among nuclei with $Z \geqslant 6$ the heavier nuclei were systematically overabundant in cosmic rays relative to the lighter ones. Some recent revisions of the solar Fe abundance (Garz *et al.*, 1969), as well as revisions in the cosmic ray data itself and in part the C and O abundances discussed earlier, have shown that the second conclusion is too simplified. The differences appear to be selective rather than systematic.

To put the discussion on the relative abundances in a perspective, let us assume that cosmic rays have their origin in the late stages of supernova evolution. If this is correct, then their abundance should reflect some average elemental abundance of energetic supernova ejecta. Furthermore, let us assume that the present composition of the sun (or meteorites) represents the solar composition $\sim 5 \times 10^9$ yr ago when the sun was born out of interstellar material and that this composition represents some average of element building processes occurring in the early history of our Galaxy. It is presently argued that this element building was much more rapid in an early stage of evolution – so that little change in the average interstellar material abundance has occurred in the last 5×10^9 yr. In such a comparison, one might expect a correspondence between the cosmic ray and solar abundances. This could be modified in a number of ways as follows: (1) The two could have a common origin as discussed above, but the cosmic rays could be preferentially accelerated in such a way as to alter the original source composition as reflected in some manner by the solar abundances. This effect might be such as to systematically alter the cosmic ray source composition (e.g. $\sim Z$), or it might, for example, depend in some way on the ionization potential of the various nuclei (Havnes, 1971). The ratios we have compiled in Table V show no systematic correlation with ionization potential, as in the data discussed by Havnes. (2) The two could have a common origin, but the cosmic rays could be created at a different time in the chemical evolution than the average of the bulk of the ejected mass (solar abundances). If we examine the relative composition data with this point in mind, some interesting features may be discerned. First of all, the C/O ratio in cosmic rays is much different than in solar material. This is directly related to the fact that C, N, and O are all underabundant in cosmic rays relative

to Fe as compared with solar abundances and might suggest, for example, that C and O burning have proceeded further to produce the cosmic ray composition. There are differences in the cosmic and solar abundances of the so-called α-particle nuclei, Ne, Mg, Si and S which are clearly present, and which also seem to require somewhat different evolutionary features. It is also interesting that Ne and A are very underabundant in cosmic rays relative to the sun. (3) The two species of nuclei do not have a common origin in supernova at all, but are only casually related. Such a conclusion requires the existence of a further class of objects in which nucleo-synthesis of heavy elements occurs, and it does not seem possible to proceed with this approach further until our ideas of nucleo-synthesis in massive objects have been developed further. In this connection, we should close by noting that recent very important advances have been made in our quantitative understanding of this nucleo-synthesis, particularly for the cases of explosive Carbon, Oxygen, and Silicon burning (Clayton, 1971; Arnett, 1971). Most of the detailed comparisons of the predicted abundances have been made with solar or stellar abundances, however, and it is not clear how the cosmic ray abundance measurements should be fitted into such studies. It does seem that the cosmic ray source composition data has reached a level of precision that such comparisons can be fruitful. This will be greatly enhanced when mass measurements of the cosmic rays can be made.

11. Summary and Conclusions

In this paper we report measurements of the chemical composition of cosmic rays at high and low energies obtained on balloons using two new scintillation counter telescopes of large area and of greatly improved charge resolution and background suppression. The chemical composition we deduce at the top of the atmosphere has a number of differences from earlier work. The principal conclusions of a detailed study of this chemical composition are:

(1) The vacuum path length distributions of cosmic ray trajectories must not differ greatly from $N(X) \sim \exp(-XX_e)$ if the observed abundances of secondary nuclei at the top of the atmosphere are to be reproduced by interstellar fragmentation.

(2) For propagation models in which $N(X)$ does not differ greatly from the exponential form given above, the deduced cosmic ray source abundance changes only vary slightly.

(3) The cosmic ray source composition that we deduce does not show a systematic overabundance of heavier nuclei as in some previous discussions. The differences appear to be selective, rather than systematic. Some of these differences suggest a further nuclear evolutionary history for the cosmic ray particles beyond that necessary to explain the solar abundances.

Acknowledgements

This work was sponsored by NASA under Grant NGR 30–002–052. One of the authors, SVD, is on leave from TIFR in Bombay, India.

References

Arnett, W. D.: 1971, *Astrophys. J.* **166**, 153.
Baity, W. H., Teegarden, B., Lezniak, J. A., and Webber, W. R.: 1971, *Astrophys.J.* **164**, 521.
Cameron, A. G. W.: 1969, in L. H. Ahrens (ed.), *Origin and Distribution of the Elements,* Pergamon, London, p. 125.
Cartwright, B. G., Garcia Munoz, M., and Simpson, J. A.: 1971, *12th Int. Conf. on Cosmic Rays, Hobart* **1**, 215.
Casse, M. M.: 1971, Research Report Centre D'Études Nucleaires de Saclay.
Casse, M., Koch, L., Lund, N., Meyer, J. P., Peters, B., Soutoul, A., and Tandon, S. N.: 1971, *12th Int. Conf. on Cosmic Rays, Hobart* **1**, 241.
Clayton, D. D.: 1971, *Comm. Astrophys* **3**, 13.
Cleghorn, T. F.: 1969, MS Thesis, University of Minnesota, Tech. Report CR-104.
Comstock, G. M.: 1969, *Astrophys. J.* **155**, 619.
Cowsik, R., Pal, Yash, Tandon, S. N., and Verma, R. P.: 1967, *Phys. Rev.* **158**, 1238.
Dayton, B., Lund, N., and Risbo, T.: 1970, *Acta. Phys. Hung.* **29**, *Suppl. 1*, 385.
Fichtel, C. E. and Reames, D. V.: 1968, *Phys. Rev.* **175**, 1564.
Garcia-Munoz, M. and Simpson, J. A.: 1970, *Acta. Phys. Hung.* **29**, *Suppl. 1,* 317.
Garz, T., Holweger, H., Kock, M., and Richter, J.: 1969, *Astron. Astrophys.* **2**, 446.
Gleeson, L. J. and Axford, W. I.: 1968, *Astrophys. J.* **154**, 1011.
Goldstein, M. L., Fisk, L. A., and Ramaty, R.: 1970, *Phys. Rev. Letters* **25**, 832.
Havnes, O.: 1971, *Nature* **229**, 548.
Jokipii, J. R. and Parker, E. N.: 1970, *Astrophys. J.* **160**, 735.
Lezniak, J. A. and Webber, W. R.: 1971, *J. Geophys, Res.* **76**, 1605.
Lezniak, J. A., von Rosenvinge, T. T., and Webber, W. R.: 1970, *Acta. Phys. Hung.* **29**, *Suppl. 1,* 375.
Lingenfelter, R. E., Ramaty, R., and Fisk, L. A.: 1971, *Astrophys. Letters,* **8**, 93.
Meneguzzi, M., Audouze, J., and Reeves, H.: 1971, Preprint SEP, Saclay.
Meyer, J. P.: 1971, *Conf. on Isotopic Composition, Copenhagen.*
Ormes, J. F. and Webber, W. R.: 1967, *J. Geophys. Res.* **73**, 4231.
Pacheco, J.: 1971, Preprint, Nice.
Perkins, M. A., Kristoff, J. J., Mason, G. M., and Sullivan, J. D.: 1969, *Nuc. Inst. Meth.* **68**, 149.
Price, P. B., Peterson, D. D., Fleischer, R. L., O'Ceallaigh, C., O'Sullivan, D., and Thompson, A.: 1970, *Acta. Phys. Hung.* **29**, *Suppl. 1,* 417.
Ramaty, R. and Lingenfelter, R. E.: 1971, *Conf. on Isotopic Composition, Copenhagen.*
Shapiro, M. M. and Silberberg, R.: 1970, *Ann. Rev. Nucl. Sci.* **30**, 323.
Shapiro, M. M. and Silberberg, R.: 1971, *12th Int. Conf. on Cosmic Rays, Hobart,* p. 221.
Shapiro, M. M., Silberberg, R., and Tsao, C. H.: 1970, *Acta. Phys. Hung.* **29**, *Suppl. 1,* 471.
Unsold, A. O. J.: 1969, *Science* **163**, 1015.
von Rosenvinge, T. T.: 1969, Ph.D. Thesis, University of Minnesota.
von Rosenvinge, T. T. and Webber, W. R.: 1968, *Nucl. Inst. Meth.* **66**, 119.
von Rosenvinge, T. T., Webber, W. R., and Ormes, J. F.: 1969, *Astrophys. Space Sci.* **5**, 342.
Waddington, C. J.: 1969, *Astrophys. Space Sci.* **5**, 3.
Waddington, C. J. and Freier, P. S.: 1968, *Phys. Rev.* **175**, 1649.
Waddington, C. J., Freier, P. S., and Long, C. E.: 1970, *Acta. Phys. Hung.* **29**, *Suppl. 1*, 367.
Webber, W. R. and Kish, J.: 1971, *Nucl. Inst. Meth.* (to be published).